Measuring the dynamic mechanical response of hydrated mouse bone by nanoindentation

Siddhartha Pathak[a,b,*], J. Gregory Swadener[c,d], Surya R. Kalidindi[a,e], Hayden-William Courtland[f], Karl J. Jepsen[g], Haviva M. Goldman[h]

a Department of Materials Science and Engineering, Drexel University, Philadelphia, PA 19104, USA
b EMPA, Swiss Federal Laboratory for Materials Science and Technology, Feuerwerkerstrasse 39, 3602 Thun, Switzerland
c Center for Integrated Nanotechnologies, Los Alamos National Laboratory, Los Alamos, NM 87545, USA
d Engineering Systems & Management, Aston University, Aston Triangle, Birmingham B4 7ET, UK
e Department of Mechanical Engineering and Mechanics, Drexel University, Philadelphia, PA 19104, USA
f Division of Endocrinology, Diabetes, and Bone Diseases, Mount Sinai School of Medicine, New York, NY 10029, USA
g Department of Orthopaedics, Mount Sinai School of Medicine, New York, NY 10029, USA
h Neurobiology and Anatomy, Drexel University College of Medicine, Philadelphia, PA 19129, USA

ABSTRACT

This study demonstrates a novel approach to characterizing hydrated bone's viscoelastic behavior at lamellar length scales using dynamic indentation techniques. We studied the submicron-level viscoelastic response of bone tissue from two different inbred mouse strains, A/J and B6, with known differences in whole bone and tissue-level mechanical properties. Our results show that bone having a higher collagen content or a lower mineral-to-matrix ratio demonstrates a trend towards a larger viscoelastic response. When normalized for anatomical location relative to biological growth patterns in the anteromedial (AM) cortex, bone tissue from B6 femora, known to have a lower mineral-to-matrix ratio, is shown to exhibit a significantly higher viscoelastic response compared to A/J tissue. Newer bone regions with a higher collagen content (closer to the endosteal edge of the AM cortex) showed a trend towards a larger viscoelastic response. Our study demonstrates the feasibility of this technique for analyzing local composition–property relationships in bone. Further, this technique of viscoelastic nanoindentation mapping of the bone surface at these submicron length scales is shown to be highly advantageous in studying subsurface features, such as porosity, of wet hydrated biological specimens, which are difficult to identify using other methods.

1. Introduction

Bone is a composite material whose mechanical performance is strongly dependent on the complex details of its internal hierarchical structure (Currey, 2003). At the micron length scale, the mechanical properties of bone are dominated by close interactions between its collagen fibrils and crystalline mineral components (Weiner et al., 1999). The hydroxyapatite mineral phase in bone is stiff and hard, while the organic collagen network is complaint and soft. Thus bone, especially in a hydrated condition, often exhibits both an elastic response and a time-dependent viscoelastic response (Fischer-Cripps, 2004).

The study of the viscoelastic behavior of bone, particularly at the submicron length scale, is made difficult by its structural complexity and inherent heterogeneity. In this respect, genetically inbred mouse strains, with known interstrain variability (Jepsen et al., 2001) and whole bone biomechanical properties (Jepsen et al., 2003), represent an important tool in studying the local mechanical properties of bone (Courtland et al., 2008). In particular, the two different strains of inbred mouse selected for this study, A/J and C57BL/6J (B6), have been shown to significantly differ in their matrix mineralization and whole bone brittleness (Jepsen et al., 2001, 2003; Price et al., 2005; Tommasini et al., 2005). Aided by a detailed knowledge of the growth patterns in these mouse strains (Price et al., 2005), we aim to characterize bone's dynamic mechanical properties using nanoindentation techniques, and thus provide insight into the relationship between mineral/matrix variation and tissue-level mechanical properties in bone.

Nanoindentation, with its ability to probe small material volumes in the micrometer length scale, is finding increasing application in the mechanical characterization of hierarchical structures such as bone and other biomaterials (Haque, 2003; Angker and Swain, 2006; Ebenstein and Pruitt, 2006; Gupta et al., 2006; Lewis and Nyman, 2008). However, despite the fact that most biological materials including bone are naturally hydrated in their in vivo environment, the majority of the published literature on bone indentation has been performed on dehydrated specimens embedded in epoxy or resin, mainly to facilitate sample preparation (Rho et al., 1997, 1998, 1999; Roy et al., 1999; Minary- Jolandan and Yu, 2009). Preservation and processing are known to affect the physical and mechanical properties of mineralized tissues (Broz et al., 1993; Linde and Sorensen, 1993; Gustafson et al., 1996; Lucksanasombool et al., 2001; Bembey et al., 2006a,b), and indentation studies on bone have also reported significant increases in indentation moduli after dehydration (Rho and Pharr, 1999; Bembey et al., 2006a; Mittra et al., 2006), with further increases after embedding (Bushby et al., 2004; Hoffler et al., 2005). In macroscopic dynamic mechanical tests, wet human cortical bone samples have been found to exhibit two to three times larger viscoelastic response (measured in terms of loss tangent) than their dry counterparts (Lakes et al., 1979; Yamashita et al., 2002). This emphasizes the need for testing samples that reflect bone's natural hydrated state, while avoiding prolonged dehydration during sample preparation. The surface layer of biological materials like bone is also highly susceptible to changes in the composition and pH of the storage media (Gustafson et al., 1996). Although dehydration and subsequent rehydration is known not to significantly affect the whole bone mechanical properties (Currey, 1988; Lucksanasombool et al., 2001; Nazarian et al., 2009), the effect of such procedures on the accuracy of sensitive surface-probing techniques such as nanoindentation has yet to be analyzed in detail (Balooch et al., 1998). Another important factor in obtaining reliable results from nanoindentation experiments is the careful and reproducible preparation of the specimen surfaces to be analyzed (Pathak et al., 2009b), especially for biological materials such as bone (Ho et al., 2004; Donnelly et al., 2006a; Deuschle et al., 2007). An adequate surface finish is especially difficult to obtain in the case of wet mouse bone samples, because of the small size of the specimens and the need to keep the samples hydrated during the entire sample preparation process. The surface roughness of wet biological samples is known to be greater than that of dry specimens (Habelitz et al., 2002; Bushby et al., 2004).

Most quasi-static nanoindentation data analysis methods have been predominantly associated with the calculation of the material elastic modulus and hardness values from the unloading data (Oliver and Pharr, 1992), as well as some aspects of the post-elastic behavior (Kalidindi and Pathak, 2008; Pathak et al., 2009a) using elastic contact mechanics (Hertz, 1896). A major impediment to the use of similar analyses on bone, especially under hydrated conditions, is its timedependent behavior (Fung, 1993), which can lead to ambiguity in the analysis of the load–displacement response. For example, persistent creep during the initial unloading in bone can give rise to the appearance of a negative stiffness (Briscoe et al., 1998; Klapperich et al., 2001; Feng and Ngan, 2002; Oyen and Cook, 2003), which has led several researchers to suggest various experimental approaches (Rho and Pharr, 1999; Rho et al., 1999; Roy et al., 1999; Chudoba and Richter, 2001; Bembey et al., 2006b; Tang et al., 2006) to eliminate the problem. However, rather than 'removing' this time dependence and measuring just an equilibrium modulus and hardness, in this report we focus on measuring the viscoelastic parameters of the material (bone) using dynamic nanoindentation measurements.

Various analysis techniques using instrumented indentation methods have been developed for direct analysis of material viscoelasticity (see Oyen and Cook, 2009 for a detailed review). In the method used in this work, a small oscillatory force is imposed on the indenter, and the resulting load, displacement and phase signals are monitored to calculate the elastic and viscous components of the specimen (Syed Asif et al., 2001). Commonly referred to as dynamic nanoindentation, such an approach allows the measurement of the loss tangent, which is considered a reliable measure of a material's viscous damping (Singh et al., 2008), over a wide range of frequencies. In this paper, we provide a detailed explanation of this method, including the details of the sample preparation used on the mouse femora. Using the above techniques, we then describe and compare the viscoelastic response of bone tissue obtained from the femora of two mouse strains, A/J and B6, and discuss further potential advantages of this technique in its application to bone tissue.

2. Materials and methods

2.1. Sample preparation

Samples of femora were obtained from A/J and C57BL/6J (B6) strains of inbred mice at 16 weeks of age. Following the procedure detailed in Jepsen et al. (2001), A/J and B6 mice were obtained at 4–6 weeks of age from Jackson Laboratory (Bar Harbor, ME, USA), fed a standard mouse chow (Teklad 8664; Harlan, Indianapolis, IN, USA) ad libitum, kept on a 12 h light/dark cycle, and housed with five mice per cage at the Department of Orthopaedics in Mount Sinai School of Medicine (MSSM), NY. All mice were sacrificed at 16 weeks of age at a time when the long bones are at peak bone mass (Price et al., 2005). Immediately after death, the right and left femora were harvested and cleaned of soft tissue. The femur samples were then kept immersed in a phosphate-buffered saline (PBS) solution (pH 7.4) mixed with CaCl2 (210 mg of CaCl2 per liter of PBS) (Gustafson et al., 1996), and stored frozen at -20^{o} C. Two sets of samples – 'wet' (hydrated) and 'dry' (dehydrated/embedded) – were prepared for indentation testing (see Fig. 1).

For the wet samples, care was taken to keep the femora moist with PBS solution at all times during their preparation and testing. Four samples of the right femur from each strain were chosen for testing. Samples were transported while frozen to the Bone Biology Laboratory at Drexel University College of Medicine (DUCOM). The samples were thawed and potted using an acrylic adhesive (Scotchweld DP810, McMaster Carr, Los Angeles, CA) and then sectioned transversely distal to the third trochanter using a Buehler Isomet 1000 saw (Lake Bluff, IL). Grinding and polishing procedures followed immediately. Grinding to increasingly fine sandpaper number up to 1200 grit was followed by polishing (using a Buehler Ecomet 3000, Lake Bluff, IL) with a series of napped cloths impregnated with diamond paste, finishing with a grain

size of 0.25 μm. The samples were cleaned ultrasonically after each preparation step and checked by optical microscopy to ensure a reproducible surface finish (see Fig. 1). The samples were then refrozen (soaked in PBS solution pH 7.4) and stored at −20°C. Since various stages of the sample preparation and testing were conducted in three different facilities – the mice were harvested at MSSM, the femora were potted, cut and polished at DUCOM, and the nanoindentation was conducted at the Center for Integrated Nanotechnologies (CINT) facility at Los Alamos National Laboratory (LANL), Los Alamos, NM – it required several storage (by freezing), thawing and refreezing cycles of the bones. Although storage by freezing, and thawing, testing and refreezing sequences are not expected to affect the mechanical properties of bone (Linde and Sorensen, 1993), care was taken to ensure that all of the samples tested underwent the same number of freeze–thaw cycles, in order to ensure better homogeneity of the results. Viscoelastic indentation testing was performed after thawing and conditioning the samples in PBS solution at room temperature for ∼1 h. The samples were kept submerged in PBS in a fluid cell during the entire test duration in order to maintain hydration.

For comparison, another set of samples (right femora from a different group of the same mouse strains) were prepared for testing in the dry condition (see schematic in Fig. 1). These samples were fixed in 70% ethanol, dehydrated in ascending grades of ethanol and embedded in polymethylmethacrylate (PMMA). The bone surface was prepared for nanoindentation testing by grinding with increasingly fine sandpapers up to 1200 grit, and polishing by means of a series of napped cloths impregnated with diamond paste, finishing with a grain size of 0.05 μm. The samples were cleansed in a distilled water ultrasonic bath after each successive step. The dry femur sections were imaged using a Leica TCS SP2 Laser Scanning Spectral Confocal Microscope (Leica Microsystems Inc., Bannockburn, IL), then carbon coated and imaged using backscattered electron microscopy (BSEM) (following the methods of Goldman et al. (2003)) with an Amray 1845 field emission scanning electron microscope (FE-SEM) with 4pi digital interface (SEMTech, North Billerica, MA). Quantitative data from these images are not reported in this paper—rather the images are used here for illustrative purposes only.

2.2. Areas of interest

As stated before, one of the main reasons for choosing the A/J and B6 mice strains is that their bone growth patterns are well studied and understood. At 16 weeks of age, these mouse femora are still in the state of being actively modeled (Beamer et al., 1996; Price et al., 2005), with new bone being deposited along the inner (endosteal) and outer (periosteal) surfaces, though mineralization data indicate that interstrain differences have clearly been established by this time. Specifically, these mice experience a particular pattern of cortical drift (Enlow, 1963) (see Fig. 2) in which new bone is deposited on the endosteal (inner) surface along the anteromedial (AM) cortex and periosteally along the postero-lateral cortex. Owing to this growth pattern, newly formed bone near these surfaces has been shown to have a lower mineral-tomatrix ratio and different chemical composition (Courtland et al., 2008, 2009; Pathak, 2009), relative to intracortical, older bone matrix. We expect that the viscoelastic properties will differ between these regions as a consequence.

This pattern of cortical drift allows us to select the AM cortex of the bone for our viscoelastic nanoindentation experiments as a representative region where we can readily identify areas of older and newer bone deposition. As visualized in backscattered electron microscopy (Fig. 2), and quantified by Fourier transform infra-red (FTIR) imaging (Courtland et al., 2008) and Raman spectroscopy (Pathak, 2009), newly formed bone matrix with lower mineral-to-matrix ratio is present closer to the endosteal surface, while more mature bone with higher mineral-to-matrix ratio is located deeper into the cortex. Starting at 5 μm from the endosteal surface and proceeding periosteally, three rows of indentations (distance between

successive rows 10 μm), with ten indents in each row spaced 10 μm apart, were made on each sample, as shown in Fig. 2. This generated viscoelastic indentation maps over a 20 μm× 90 μm area of the sample.

A two-way analysis of variance was used to examine the statistical significance of the viscoelastic response on the two mouse strains at different locations along the AM cortex. The small sample size used in this study (*n* = 4 per strain) limits the power of our statistical analysis; therefore, most of the results are discussed as trends across the two mouse strains.

2.3. Dynamic nanoindentation

The microscale dynamic nanoindentation tests were performed using the 'frequency-sweep' mode of the nano- DMA R ▪ (Dynamic Mechanical Analysis) software in the Hysitron Triboscope R ▪ (Hysitron Inc., Minneapolis, MN, USA) located at the CINT facility in LANL. In this mode, the applied load is specified, and the probe is oscillated across a range of frequencies (Syed Asif et al., 2001). By measuring the resultant load amplitude, displacement amplitude and the phase lag during the test, the nano-DMA technique allows the calculation of the loss modulus, storage modulus and tan δ. Assuming linear viscoelasticity, the frequency-dependent dynamic response of the material can be ascertained using the following equations:

$$tan\delta = \frac{E\prime}{E\prime\prime} = \frac{\omega C_S}{k_S}, E' = \frac{k_S\sqrt{\pi}}{2\sqrt{A_C}}, E'' = \frac{\omega C_S}{2\sqrt{A_C}} \quad (1)$$

where E' and E'' denote the storage and loss moduli, ω is the frequency of the applied force, k_S and C_S are the sample stiffness and damping coefficients, respectively, and A_C is the projected contact area of the indent on the surface of the specimen.

Note, however, that the estimation of A_C in Eq. (1) is not straightforward. The most common approach has been to calibrate A_C using measurements on samples with known moduli (Oliver and Pharr, 1992) or results from simulations (Bouzakis and Michailidis, 2006). This approach implicitly assumes that the calibration function developed for A_C is independent of the material being indented. This is unlikely, because the inherent response of the material should play an important role in determining the contact geometry. Moreover, most commercial nanoindentation instruments perform poorly when trying to detect the surface of soft materials (Kalidindi and Pathak, 2008; Pathak et al., 2009a) – the accuracy can vary anywhere from ~2 nm (Oliver and Pharr, 2004) to ~30 nm. (Deuschle et al., 2007) – and the problem is especially exacerbated in hydrated specimens (Franke et al., 2007; Kaufman and Klapperich, 2009). Since the accuracy in the calculation of A_C is directly related to the accuracy of finding the surface, this causes significant uncertainty in the calculation of the values of loss and storage moduli from Eq. (1). On the other hand, calculation of tan δ is independent of A_C, and it is ideally suited as a measure of the viscoelasticity of the indented material (Singh et al., 2008).

For wet sample testing, the indenter tip oscillations take place inside the PBS medium (instead of air). In order to account for this change in the test environment, the machine calibrations were conducted with the indenter tip being submerged in the PBS solution. A frequency range from 10 to 200 Hz was chosen for this work, with the displacement amplitudes and phase responses being recorded at 12 equally distributed frequency intervals. Although the Hysitron Triboscope R◯ indenter machine has a larger frequency range available for viscoelastic testing, the noise levels in the tests were found to be substantially higher at oscillations greater than 200 Hz inside the PBS solution. The noise level in the machine (around 0.03 tan δ) was determined by conducting frequency sweeps in non-viscoelastic materials such as aluminum and tungsten.

The choice of the indenter tip shape also plays an important role in the measurement of viscoelastic properties of a hydrated specimen. In this respect, spherical tips are ideal for indenting soft polymers and tissues (Syed Asif et al., 2001; Fischer-Cripps, 2004; Ebenstein and Pruitt, 2006) due to their relatively smoother stress fields (compared to sharper indenters (Pathak et al., 2008)) and lower sensitivity to alignment problems (compared to flat punches (Herbert et al., 2008; Wright and Nix, 2009)). Thus, fluid tips (specialized tips with long shafts to minimize the meniscus forces acting on the indenter (Rho and Pharr, 1999)) with spherical probes of radius 1 and 20 μm at the end were used in this work.

In this work, the indenter tip was held for 2 min at the applied load in order to dissipate any creep effects before starting the probe oscillations. The applied AC load for each test was adjusted to ensure a displacement amplitude of ~2 nm, at a nominal depth of ~200 nm inside the material. The choice of this indentation depth ensured that the contact area between the sample and the sphero-conical indenter tip stayed in the spherical regime, which extends to a depth of around 30% of the indenter radius for a 90^{o} indenter cone geometry. Similar tests were also done on dry polycarbonate samples with known values of tan δ to validate the accuracy of the method. The 'imaging' mode of the Hysitron Triboscope® was employed in this work. This enables the topography of the sample to be readily visualized and facilitates the exact placement of the indent on the region of interest (Syed Asif et al., 2001), especially when the sample surface is submerged in liquid.

3. Results

A comparison of the viscoelastic nanoindentation response in both wet and dry conditions is shown in Fig. 3. Notice the smaller tan δ values in the dehydrated bone relative to the hydrated bone. Fig. 4 shows the variation in the tan δ values in the wet condition as a function of frequency across a row of indents starting from 5 μm of the endosteal edge in the AM cortex; two samples of each strain are shown as examples. The following trends are evident from these plots. First, no particular frequency dependence within this frequency range is seen. Second, at a similar distance from the endosteal edge, the B6 mice demonstrate larger values of tan δ than the A/J mice, a trend that suggests a larger viscoelastic response for the B6 mice strain at a similar distance into the cortex. Finally, in both mouse strains, there is a trend towards larger values of tan δ close to the endosteal edge, with the values decreasing progressively as the indenter moves away from the edge.

These trends are illustrated further in Figs. 5 and 6. Fig. 5 illustrates two-dimensional surface maps of tan δ over a region of 20 μm×70 μm close to the endosteal edge of the AM cortex at a representative (mid-range) frequency of 101 Hz. Results from four 'wet' samples of the B6 strain and three of the A/J strain are shown in this figure (the fourth A/J sample is excluded from this figure due to the presence of a large pore in the scanned area). Fig. 6 presents the average and standard deviations of the tan δ values from Fig. 5 over all of the measured indentation locations in 'wet' A/J and B6 at a frequency of 101 Hz. Again, at a similar distance from the endosteal edge, the B6 sample is seen to demonstrate a larger average value of tan δ than the A/J sample. The tan δ values across both strains also tend to decrease as the indenter moves away from the endosteal edge; however, the tan δ values did not show any significant differences between the different test locations within a particular strain of mice.

Two-way analysis of variance for the two mouse strains and eight locations (distance from the endosteal edge, Fig. 6) were calculated for data at 29, 101 and 172 Hz. The results indicate that the mouse strain and locations are not interrelated ($p > 0.5$): there is a statistically significant difference between strains ($p < 0.0001$), but there is no statistically significant difference between locations ($p > 0.1$). In pair-wise

comparisons only one location – at a distance of 5 μm from the endosteal edge – shows a statistically significant difference ($p = 0.028$) between the two strains. A larger sample size would likely improve our ability to interpret these results statistically.

4. Discussion

As seen from Fig. 3, hydrated 'wet' mouse bone displays a clear viscous response (larger values of tan δ), whereas dry bone samples do not show any appreciable viscoelasticity (low values of tan δ which are comparable to the noise level of the machine). These results underline the need for testing bone in the hydrated state.

Our results also demonstrate that the tan δ values for the mouse femora are consistent throughout the range of tested frequencies (10–200 Hz), although a further frequency dependence outside of this range cannot be ruled out. This trend is in contrast to that reported by Donnelly et al. (2006b), who found a decrease in values of the loss tangent tan δ with increasing test frequencies, and the review by Lewis and Nyman (2008), where an opposite trend of increasing values of tan δ with higher frequencies is reported. Both of the above two studies were done in the 0–200 Hz frequency range. These discrepancies may stem from the different animals studied in these studies (human vertebrae in Donnelly et al. (2006b) and bovine plexiform bone in Lewis and Nyman (2008)), as compared to the mouse femora studied in this work. Also, since the experiments performed by Donnelly et al. (2006b) were conducted on dry dehydrated bone samples, the tan δ values measured in their work are also much lower (tan δ ranging from 0.02 to 0.07) than the values obtained on our mouse femur samples, and as such are comparable to the tan δ values for dehydrated bone shown in Fig. 3. The experimental details for the results shown by Lewis and Nyman (2008) were not provided in their review paper, and hence a direct comparison with this work is currently not possible.

The significant difference in viscoelastic response between the two tested mouse strains can be explained relative to our existing knowledge of the growth, morphology and local composition of these femora. It is known that, while the A/J femora have a smaller diameter and correspondingly a smaller moment of inertia compared to B6 (see Fig. 5), they do not differ in their cortical areas (Jepsen et al., 2001, 2003). However, instead of a less structurally efficient structure as one would expect (if the bone compositions were identical across the two mouse strains), the A/J femora are found to possess similar overall stiffness and strength values (Jepsen et al., 2001). A/J bones appear to have biologically coupled a change in bone quality to their bone morphology in order to satisfy the imposed mechanical demands (Jepsen et al., 2003). Specifically, A/J mouse bones have a significantly higher ash content (Jepsen et al., 2003) and mineral-to-matrix ratio as measured by FTIR (Courtland et al., 2008) and Raman spectroscopy (Patel, 2007; Pathak, 2009) relative to B6 mouse bones. Moreover, spherical nanoindentation performed on dry samples (Pathak, 2009) demonstrated a corresponding trend towards larger modulus values (~30 GPa) for the A/J mice at the tissue level, compared to B6 (~22 GPa). Using the wet samples, we are now able to preliminarily demonstrate that the more highly mineralized and thus less collagenous tissue matrix also results in a smaller viscoelastic response in the A/J mice. Our use of the inbred mouse model in this study highlights the potential of this technique for elucidating local compositional and property relationships in bone, and understanding how such relationships might affect whole bone performance. Future studies, using larger and more appropriate sample sizes, will allow us to pursue these biological relationships further.

Our study demonstrated that although there were few significant differences in tan δ between our test locations (from endosteal to periosteal surfaces), there was a trend towards smaller values of tan δ in more intracortical bone areas (see Fig. 4). A larger sample size would likely allow us to better understand the biological significance of these trends. Based on this preliminary data, it is likely that local variations demonstrated in the values of tan δ between bone regions of the same individual reflect the growth processes that regulate bone composition. Specifically,we knowthat the A/J and B6 femora are characterized by the growth pattern illustrated in Fig. 2, where, instead of a uniform expansion of the cortex around the periosteal or endosteal surfaces, growth is superimposed upon a cortical drift phenomenon. At the AM cortex (our area of investigation) this translates into a region of newer bone close to the endosteal surface, while the bone is more mature (older) as the indenter probes away from this surface. Both FTIR (Courtland et al., 2008) and Raman spectroscopy (Miller et al., 2007; Patel, 2007; Pathak, 2009) studies have demonstrated that the mineral-to-matrix Fig. 6 – Average and standard deviations of the tan δ values shown in Fig. 5 (at 101 Hz frequency) as measured from the endosteal edge of both A/J and B6 femora in the 'wet' condition. ratio increase as bone matures from the endosteal surface to more intracortical regions. Since hydrated bone owes its remarkable viscoelasticity to the collagen fibrils in the bone matrix (Fois et al., 2001; Jepsen et al., 2001), the trend towards larger tan δ data near the endosteal surface supports a direct relationship between larger viscoelastic response and lower mineral-to-matrix ratio, and the decrease in the values of tan δ away from the endosteal edge is indicative of the higher degree of maturity of the bone in this region. However, owing to the fact that these spectroscopic methods are applicable only on dry samples, the exact composition at the indent locations in the wet samples could not be measured in this study.

In conclusion, the reduced values of tan δ for the 'wet' A/J mouse femora can be inferred to relate to the higher mineral (and less collagen) content in these mice, as compared to the B6 mice (Jepsen et al., 2001). The B6 mouse femora, having a higher comparative collagen content, demonstrate a trend towards larger viscoelastic response (Fig. 6). The analysis presented here represents a first step in quantifying the viscoelastic response of wet bone samples as a function of test location along the bone matrix. The trends in tan δ variation between test locations suggests a local relationship between bone mineralization/maturity and viscoelasticity in these mouse femora, but further studies with larger sample sizes will be needed to explore this further. A further utility of viscoelastic mapping of the surface is illustrated in Fig. 7. In this figure the values of tan δ were used to map out a subsurface pore in the wet A/J femur bone sample that is characterized by a larger viscous response. As pores below the bone surface of this length scale are very difficult to identify in the wet condition, the ability to locate pores using tan δ values could be an important tool for studying pore features and distributions in these samples. For instance, it would be possible to readily correlate details of local porosity (e.g., osteocyte lacunae, primary vascular canals, Haversian canals) and local tissue behavior in order to study the effects of aging and disease on non-dehydrated specimens.

Conflict of interest statement

None of the authors have any financial or personal relationships with other people or organizations that could inappropriately influence the quality of the work presented in this manuscript.

Acknowledgements

This work was supported by grants from the National Institutes of Health (NIH AR044927). S.P. wishes to acknowledge the support from the 2007 Sigma Xi Grants-in-Aid of Research (GIAR) program and the 2007 Center for Integrated Nanotechnologies (CINT) user proposal grant for use of facilities at the Los Alamos National Laboratory, Los Alamos, NM. Thanks also to Phil Nasser at MSSM for assistance with sample preparation, and to Ryan J. Stromberg at Hysitron Inc. for help with the nano-DMA® technique.

R E F E R E N C E S

Angker, L., Swain, M.V., 2006. Nanoindentation: application to dental hard tissue investigations. Journal of Materials Research 21 (8), 1893–1905.

Balooch, M., Wu-Magidi, I.C., Balazs, A., Lundkvist, A.S., Marshall, S.J., Marshall, G.W., Siekhaus, W.J., Kinney, J.H., 1998. Viscoelastic properties of demineralized human dentin measured in water with atomic force microscope (AFM)-based indentation. Journal of Biomedical Materials Research 40 (4), 539–544.

Beamer, W.G., Donahue, L.R., Rosen, C.J., Baylink, D.J., 1996. Genetic variability in adult bone density among inbred strains of mice. Bone 18 (5), 397–403. Bembey, A.K., Bushby, J., Boyde, A., Ferguson, V.L., Oyen, M.L., 2006a. Hydration effects on the micro-mechanical properties of bone. Journal of Materials Research 21 (8), 1962–1968.

Bembey, A.K., Oyen, M.L., Bushby, A.J., Boyde, A., 2006b. Viscoelastic properties of bone as a function of hydration state

determined by nanoindentation. Philosophical Magazine 86 (33–35), 5691–5703 (special issue).

Bouzakis, K.D., Michailidis, N., 2006. Indenter surface area and hardness determination by means of a FEM-supported simulation of nanoindentation. Thin Solid Films 494 (1–2), 155–160.

Briscoe, B.J., Fiori, L., Pelillo, E., 1998. Nano-indentation of polymeric surfaces. Journal of Physics D (Applied Physics) 31 (19), 2395–2405.

Broz, J.J., Simske, S.J., Greenberg, A.R., Luttges, M.W., 1993. Effects of rehydration state on the flexural properties of whole mouse long bones. Transactions of the ASME. Journal of Biomechanical Engineering 115 (4A), 447–449.

Bushby, A.J., Ferguson, V.L., Boyde, A., 2004. Nanoindentation of bone: comparison of specimens tested in liquid and embedded in polymethylmethacrylate. Journal of Materials Research 19 (1), 249–259.

Chudoba, T., Richter, E., 2001. Investigation of creep behaviour under load during indentation experiments and its influence on hardness and modulus results. Surface & Coatings Technology 148 (2–3), 191–198. Courtland, H.W., Nasser, P., Goldstone, A.B., Spevak, L., Boskey,

A.L., Jepsen, K.J., 2008. Fourier transform infrared imaging microspectroscopy and tissue-level mechanical testing reveal intraspecies variation in mouse bone mineral and matrix composition. Calcified Tissue International 83 (5), 342–353.

Pathak, S., 2009. Development and validation of a novel data analysis procedure for spherical nanoindentation. Doctor of Philosophy. Drexel University, Philadelphia, PA.

Pathak, S., Kalidindi, S.R., Moser, B., Klemenz, C., Orlovskaya, N., 2008. Analyzing indentation behavior of LaGaO3 single crystals using sharp indenters. Journal of the European Ceramic Society 28 (10), 2039–2047.

Pathak, S., Shaffer, J., Kalidindi, S.R., 2009a. Determination of an effective zero-point and extraction of indentation stress–strain curves without the continuous stiffness measurement signal. Scripta Materialia 60 (6), 439–442.

Pathak, S., Stojakovic, D., Doherty, R., Kalidindi, S.R., 2009b. Importance of surface preparation on the nano-indentation stress–strain curves measured in metals. Journal of Materials Research—Focus Issue on Indentation Methods in Advanced Materials Research 24 (3), 1142–1155.

Price, C., Herman, B.C., Lufkin, T., Goldman, H.M., Jepsen, K.J., 2005. Genetic variation in bone growth patterns defines adult mouse bone fragility. Journal of Bone and Mineral Research 20 (11), 1983–1991.

Rho, J.-Y., Kuhn-Spearing, L., Zioupos, P., 1998. Mechanical properties and the hierarchical structure of bone. Medical Engineering & Physics 20 (2), 92–102.

Rho, J.-Y., Pharr, G.M., 1999. Effects of drying on the mechanical properties of bovine femur measured by nanoindentation. Journal of Materials Science: Materials in Medicine 10 (8), 485–488.

Rho, J.Y., Tsui, T.Y., Pharr, G.M., 1997. Elastic properties of human cortical and trabecular lamellar bone measured by nanoindentation. Biomaterials 18 (20), 1325–1330.

Rho, J.Y., Zioupos, P., Currey, J.D., Pharr, G.M., 1999. Variations in the individual thick lamellar properties within osteons by nanoindentation. Bone 25 (3), 295–300.

Roy, M.E., Rho, J.Y., Tsui, T.Y., Evans, N.D., Pharr, G.M., 1999. Mechanical and morphological variation of the human lumbar vertebral cortical and trabecular bone. Journal of Biomedical Materials Research 44 (2), 191–197.

Singh, S.P., Smith, J.F., Singh, R.P., 2008. Characterization of the damping behavior of a nanoindentation instrument for carrying out dynamic experiments. Experimental Mechanics 48 (5), 571–583.

Syed Asif, S.A., Wahl, K.J., Colton, R.J., Warren, O.L., 2001. Quantitative imaging of nanoscale mechanical properties

using hybrid nanoindentation and force modulation. Journal of Applied Physics 90 (3), 1192.

Tang, B., Ngan, A.H.W., Lu, W.W., 2006. Viscoelastic effects during depth-sensing indentation of cortical bone tissues. Philosophical Magazine 86 (33–35), 5653–5666 (special issue).

Tommasini, S.M., Morgan, T.G., van der Meulen, M., Jepsen, K.J., 2005. Genetic variation in structure–function relationships for the inbred mouse lumbar vertebral body. Journal of Bone and Mineral Research 20 (5), 817–827.

Weiner, S., Traub, W., Wagner, H.D., 1999. Lamellar bone: structure–function relations. Journal of Structural Biology 126 (3), 241–255.

Wright, W.J., Nix, W.D., 2009. Storage and loss stiffnesses and moduli as determined by dynamic nanoindentation. Journal of Materials Research 24 (3), 863–871.

Yamashita, J., Li, X., Furman, B.R., Ralph Rawls, H., Wang, X., Mauli Agrawal, C., 2002. Collagen and bone viscoelasticity: a dynamic mechanical analysis. Journal of Biomedical Materials Research 63 (1), 31–36.

List of Figure Captions

Fig. 1. Flow diagram for the procedure for preparation of ‘dry’ dehydrated/embedded and ‘wet’ hydrated mouse bone samples for viscoelastic indentation testing.

Fig. 2. Left: Schematic representation showing the sectioning of mouse femora transversely distal to the third trochanter. Middle: During post-natal growth, bone is deposited (double arrows) and resorbed (single arrows) at different sites around this region of the femoral cortex, resulting in a net cortical drift (large arrow), as shown in this BSEM image with superimposed confocal image demonstrating fluorescent labeling of newly formed bone. Right: Spherical nanoindents at the antero-medial (AM) cortex thus probe newer bone closer to the endosteal edge while the bone is more mature away from this surface, as seen in this BSEM image. Three rows of indentations (shown in schematic) were performed on each sample.

Fig. 3. Comparison of the viscoelastic response of ‘wet’ (hydrated) and ‘dry’ (dehydrated/embedded) A/J mouse bone.

Fig. 4. Variation of tan δ values in the ‘wet’ femur samples as a function of the frequency imposed on the 1 μm radius spherical indenter tip. Representative rows at the endosteal edge of the AM cortex for two samples of (a) the B6 mouse strain and (b) the A/J mouse strain are shown as examples.

Fig. 5. Two-dimensional surface maps of **tan** δ values at a representative mid-range frequency of 101 Hz across a **20** μ**m**× **70** μ**m** region close to the endosteal edge of the AM cortex in (a) four B6 samples and (b) three A/J mouse samples in the ‘wet’ condition. Note the smaller map size of the second B6 sample. The mouse femur sections were imaged using BSEM following the techniques described by Goldman et al. (2003).

Fig. 6. Average and standard deviations of the tan δ values shown in Fig. 5 (at 101 Hz frequency) as measured from the endosteal edge of both A/J and B6 femora in the ‘wet’ condition.

Fig. 7. A two-dimensional map of tan δ values across a 20 × 70 μm region in a ‘wet’ A/J mouse femur. The higher values of tan δ towards the middle of the mapped region were identified as a subsurface pore in the bone.

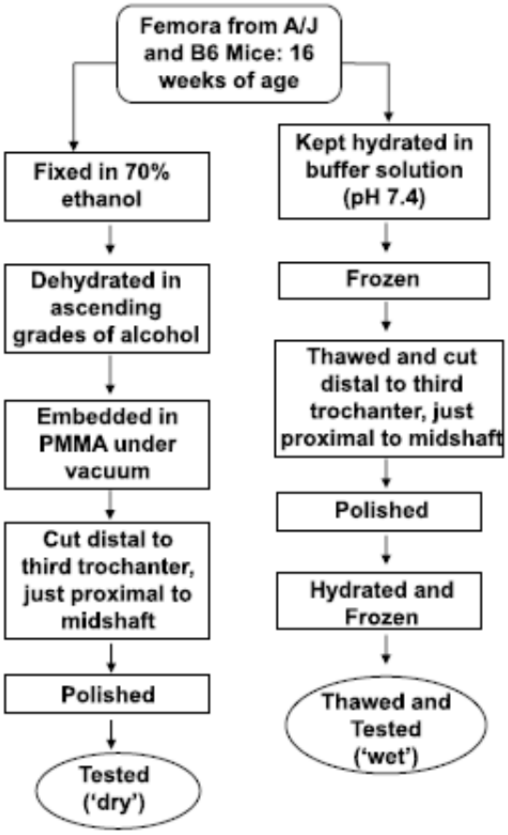

Fig. 1. Flow diagram for the procedure for preparation of ‘dry’ dehydrated/embedded and ‘wet’ hydrated mouse bone samples for viscoelastic indentation testing.

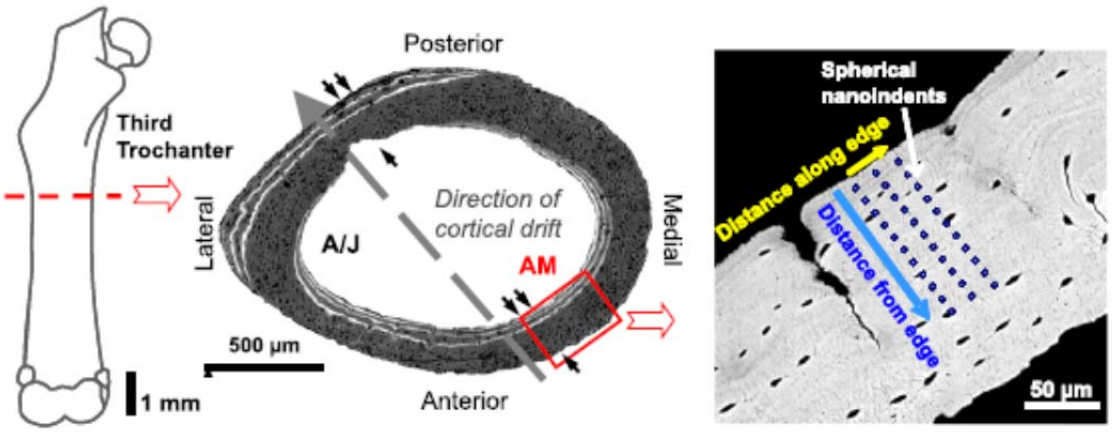

Fig. 2. Left: Schematic representation showing the sectioning of mouse femora transversely distal to the third trochanter. Middle: During post-natal growth, bone is deposited (double arrows) and resorbed (single arrows) at different sites around this region of the femoral cortex, resulting in a net cortical drift (large arrow), as shown in this BSEM image with superimposed confocal image demonstrating fluorescent labeling of newly formed bone. Right: Spherical nanoindents at the antero-medial (AM) cortex thus probe newer bone closer to the endosteal edge while the bone is more mature away from this surface, as seen in this BSEM image. Three rows of indentations (shown in schematic) were performed on each sample.

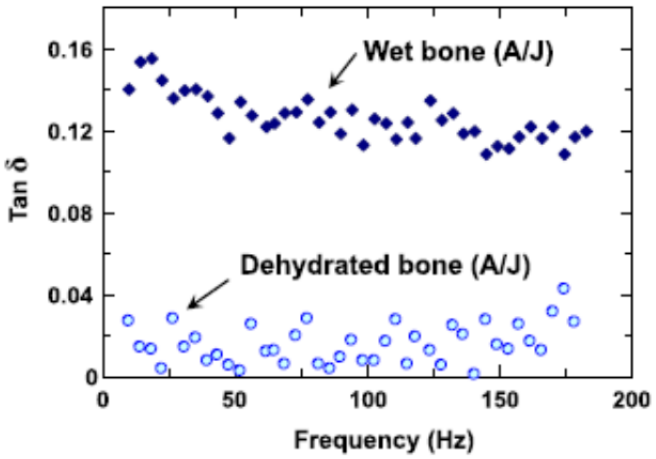

Fig. 3. Comparison of the viscoelastic response of ‘wet’ (hydrated) and ‘dry’ (dehydrated/embedded) A/J mouse bone.

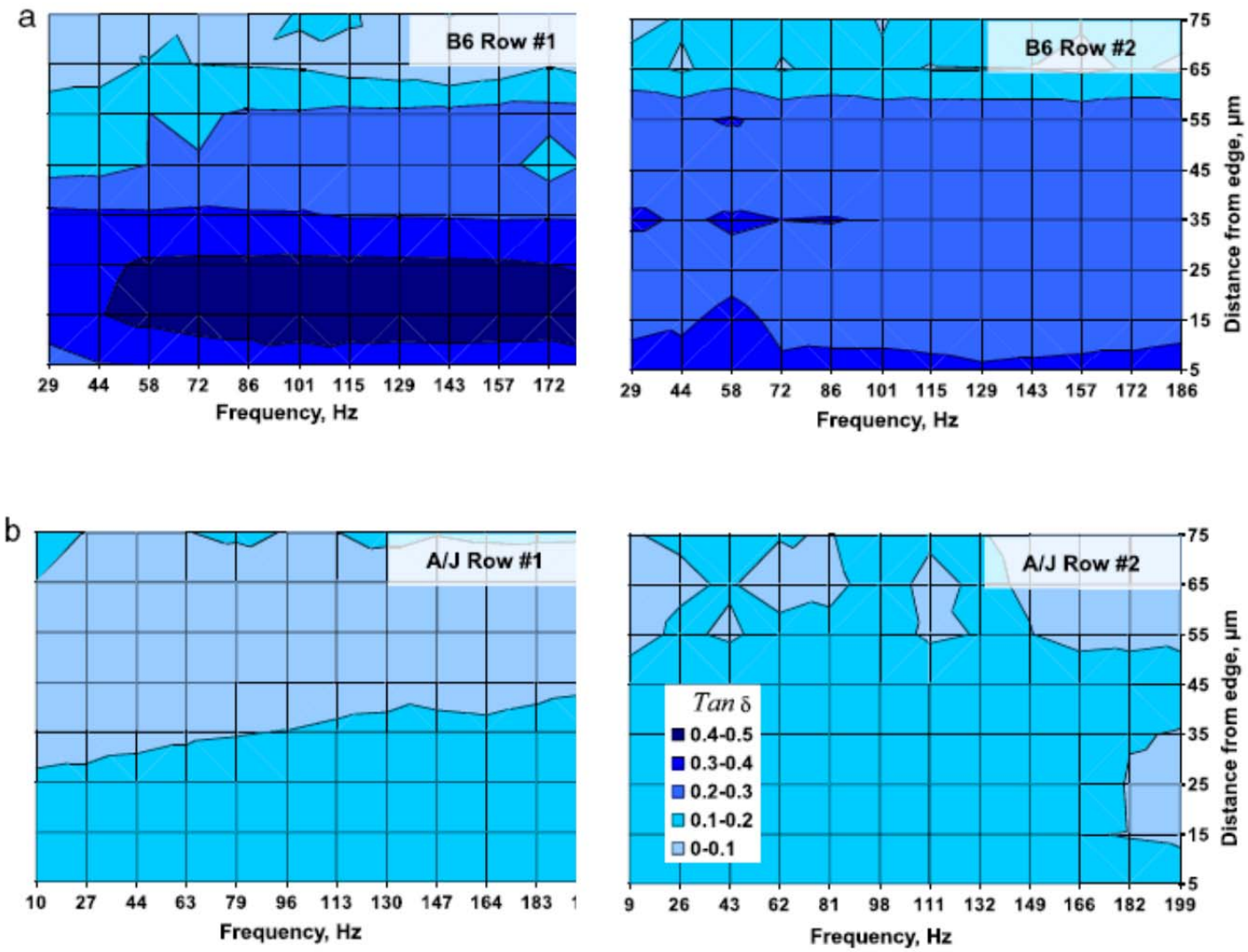

Fig. 4. Variation of tan δ values in the 'wet' femur samples as a function of the frequency imposed on the 1 µm radius spherical indenter tip. Representative rows at the endosteal edge of the AM cortex for two samples of (a) the B6 mouse strain and (b) the A/J mouse strain are shown as examples.

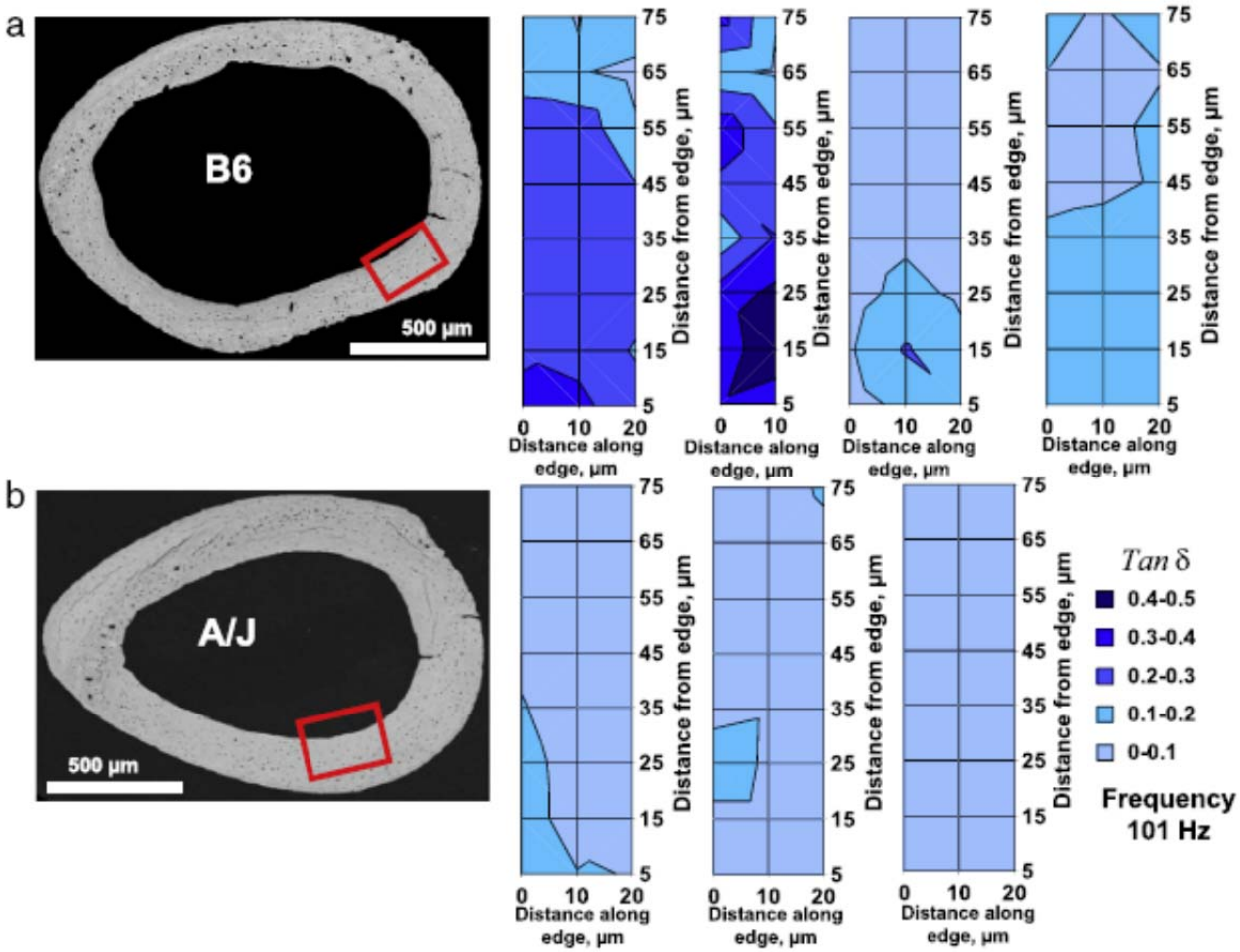

Fig. 5. Two-dimensional surface maps of **tan** δ values at a representative mid-range frequency of 101 Hz across a **20** µ**m**× **70** µ**m** region close to the endosteal edge of the AM cortex in (a) four B6 samples and (b) three A/J mouse samples in the 'wet' condition. Note the smaller map size of the second B6 sample. The mouse femur sections were imaged using BSEM following the techniques described by Goldman et al. (2003).

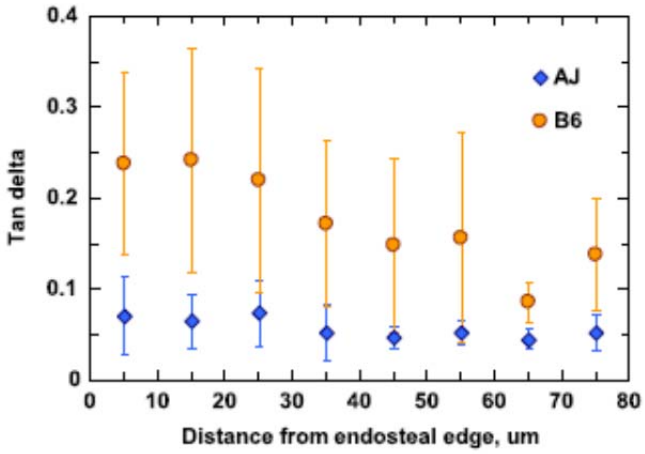

Fig. 6. Average and standard deviations of the tan δ values shown in Fig. 5 (at 101 Hz frequency) as measured from the endosteal edge of both A/J and B6 femora in the 'wet' condition.

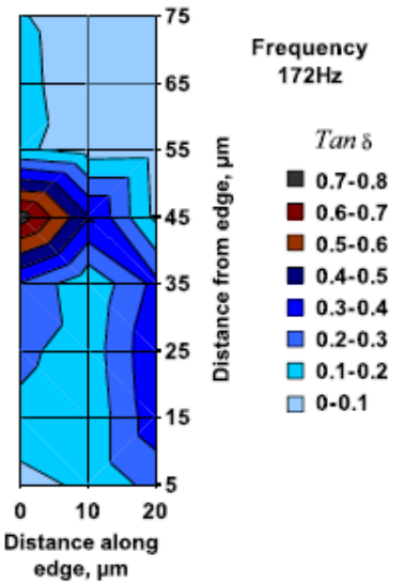

Fig. 7. A two-dimensional map of tan δ values across a 20 × 70 µm region in a ‘wet’ A/J mouse femur. The higher values of tan δ towards the middle of the mapped region were identified as a subsurface pore in the bone.